AGU PUBLICATIONS

Geophysical Research Letters

RESEARCH LETTER
10.1002/2015GL065603

Key Points:
- Geostrophic (Ekman) component dominates the interannual variations in the MOC before (after) 2006
- Satellite altimeter data can be used to estimate MOC/MHT in the South Atlantic
- The strongest MOC variations on seasonal and interannual time scales are found at 34.5°S

Correspondence to:
S. Dong,
shenfu.dong@noaa.gov

Citation:
Dong, S., G. Goni, and F. Bringas (2015), Temporal variability of the South Atlantic Meridional Overturning Circulation between 20°S and 35°S, *Geophys. Res. Lett.*, *42*, 7655–7662, doi:10.1002/2015GL065603.

Received 30 JUL 2015
Accepted 27 AUG 2015
Accepted article online 1 SEP 2015
Published online 24 SEP 2015

Temporal variability of the South Atlantic Meridional Overturning Circulation between 20°S and 35°S

Shenfu Dong[1,2], Gustavo Goni[2], and Francis Bringas[2]

[1]Cooperative Institute for Marine and Atmospheric Studies, Rosenstiel School of Marine and Atmospheric Science, University of Miami, Miami, Florida, USA, [2]Atlantic Oceanographic and Meteorological Laboratory, National Oceanic and Atmospheric Administration, Miami, Florida, USA

Abstract Altimetry-derived synthetic temperature and salinity profiles between 20°S and 34.5°S are used to estimate the Meridional Overturning Circulation (MOC) and meridional heat transport (MHT), which are assessed against estimates obtained from expendable bathythermograph (XBT) measurements. Consistent with studies from XBTs and Argo data, both the geostrophic and Ekman contributions to the MOC exhibit annual cycles and play an equal role in the MOC seasonal variations. The strongest variations on seasonal and interannual time scales in our study region are found at 34.5°S. The dominance of the geostrophic and Ekman components on the interannual variations in the MOC and MHT varies with time and latitude, with the geostrophic component being dominant during 1993–2006 and the Ekman component dominant between 2006 and 2011 at 34.5°S.

1. Introduction

The Meridional Overturning Circulation (MOC) plays a critical role in global and regional heat and freshwater budgets by carrying water properties northward and southward within individual ocean basins. The strength of the MOC has shown intense variations on time scales ranging from daily to longer term, which vary with latitude [e.g., *Cunningham et al.*, 2007; *Dong et al.*, 2009; *Zhang et al.*, 2011; *Meinen et al.*, 2013; *Smeed et al.*, 2014]. These variations in the MOC can have a pronounced impact on a variety of important climate phenomena, including Atlantic hurricane activity, precipitation and air temperature variability over North America and western Europe, and changes in African and Indian monsoon rainfall [e.g., *Enfield et al.*, 2001; *Vellinga and Wood*, 2002; *Sutton and Hodson*, 2005; *Zhang and Delworth*, 2006]. Quantifying MOC changes over time and understanding its underlying mechanisms are, therefore, crucial for improving our knowledge of how the climate system functions and for assessing climate models and future climate change.

A comprehensive MOC observing system is needed to gain a more complete understanding of its behavior. The majority of efforts to understand and measure MOC variability is focused on the North Atlantic. This is primarily because the high-latitude North Atlantic is the sole supplier of the North Atlantic Deep Water (NADW), which has been hypothesized to be a driver for the long-term MOC fluctuations [e.g., *Stommel*, 1961; *Weaver and Hughes*, 1992; *Stouffer et al.*, 2006]. However, the formation rate of NADW is believed to be influenced by the Southern Hemisphere westerlies through changes in the northward Ekman transport and interocean exchanges [e.g., *Toggweiler and Samuels*, 1993, 1995; *Sijp and England*, 2008, 2009]. Indeed, recent studies have suggested the possibility of a southern origin of the anomalous MOC and meridional heat transport (MHT) in the Atlantic, through changes in the transport of warm/salty waters from the Indian Ocean into the South Atlantic basin [e.g., *Biastoch et al.* 2008; *Lee et al.* 2011; *Kelly et al.*, 2014]. This possibility clearly manifests the importance of understanding the South Atlantic MOC (SAMOC).

Observations in the South Atlantic have been historically sparse both in space and time compared to the North Atlantic. Previous and current studies of the SAMOC are mostly focused on 34.5°S. Data from a high-density expendable bathythermograph (XBT) transect have provided the first time series of the SAMOC and MHT, on a quarterly basis since its implementation in 2002 [*Dong et al.*, 2009; *Garzoli et al.*, 2013]. More recent studies [e.g., *Meinen et al.*, 2013] used two boundary arrays of inverted echo sounders deployed along 34.5°S and found that much of the MOC variability in the 20 month record (March 2009 to December 2010) occurs at periods shorter than 100 days.

The goal of this study is to enhance our understanding of the MOC and MHT variability in the South Atlantic, in particular of changes on seasonal to interannual time scales. To accomplish this, sea surface height measurements from satellite altimetry, combined with in situ measurements, are used to estimate the

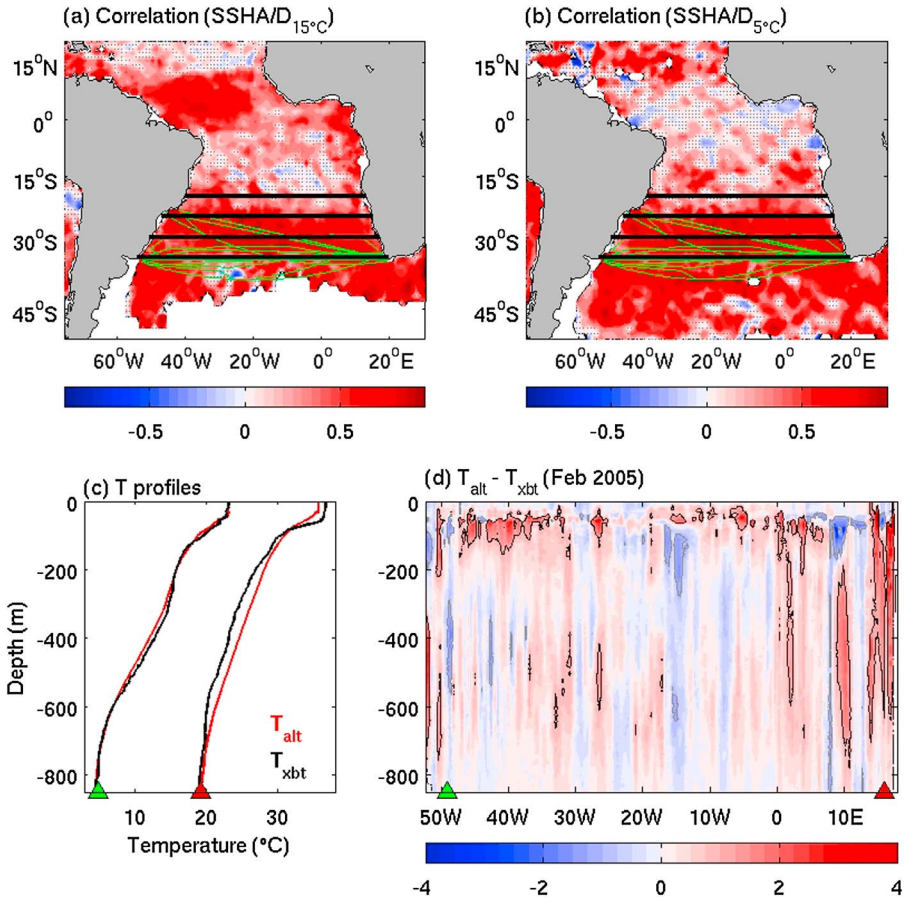

Figure 1. Correlations between SSHA and isothermal depths for (a) 15°C and (b) 5°C. Green lines show the AX18 transect locations. Dotted areas indicate where the correlations are insignificant. (c) Examples of the temperature profiles close to the boundaries and (d) temperature differences between altimeter derived and observed from XBTs for the February 2005 transect along 34.5°S. The corresponding locations for the profiles in Figure 1c are indicated by triangles in Figure 1d. Note that the profiles close to the eastern boundary (red triangles) in Figure 1c are shifted by 15°C in order to separate the two examples. Units for Figures 1c and 1d are in degree Celsius.

MOC and MHT in the South Atlantic. Of particular interest is to assess how well altimetry can be used to investigate the spatial and temporal variability of the MOC and MHT and how the contributions of the density and wind fields to the MOC and MHT change with time and with latitude.

2. Data and Methodology

The main data set used in this study corresponds to the satellite altimetry sea surface height anomalies (SSHA) from Archiving, Validation, and Interpretation of Satellite Oceanographic data [*Ducet et al*. 2000] and to temperature and salinity (T/S) profiles from the Global Temperature and Salinity Profile Program (GTSPP) [*Sun et al*., 2010]. The GTSPP archives T/S profiles from a suite of sources, including Argo floats, XBTs, mechanical bathythermographs, CTDs (conductivity-temperature-depth sensors), buoys, and bottle samplers. Consistent with previous studies [e.g., *Goni et al*., 1996, 2011; *Mayer et al*., 2001; *Dong et al*., 2007], analysis of SSHA and temperature profiles in the South Atlantic shows large correlations between SSHA and the depth of given isotherms (D_T) below the surface south of 20°S (Figures 1a and 1b), in particular below the main thermocline. These correlations allow to build linear relationships between D_T and SSHA, $D_T = \alpha + \beta \times \text{SSHA}$. The regression coefficients (α and β) at each 1°×1° grid were derived for every 1° of temperature between 3°C and 28°C using collocated SSHA and D_T that were obtained during the period 1993–2013. The collocations were done by interpolating the weekly gridded (1/4°×1/4°) SSHA into the location and time of each temperature profile. In total, approximately 42,000 profiles were used to construct these regressions, with 55% corresponding to Argo floats, 30% to XBTs,

13% to CTDs, and the rest corresponding mostly to underwater gliders and station data. Weekly synthetic temperature profiles in the upper ocean at each altimetry grid location were then generated from the gridded SSHA data using these statistical relationships. The sea surface temperature (SST) for each synthetic profile was obtained from the daily microwave optimally interpolated SST product with 25 km resolution for the period 1998 to 2011 and from the advanced very high resolution radiometer for the period 1993–1997.

Since the synthetic profiles and corresponding MOC/MHT estimates were evaluated against results from XBT measurements (section 3), we tested the impact of the XBTs on the statistical relationships between D_T and SSHA. The regression coefficients derived with and without XBT measurements are comparable, within the 95% significance interval. Therefore, excluding the XBTs in the regression analysis did not influence the evaluation of the methodology presented in section 3.

Following the methodology used to compute the MOC/MHT at 34.5°S using XBT measurements [*Baringer and Garzoli*, 2007], salinity profiles were generated using the synthetic temperature profiles and historical T/S relationships. Although these synthetic profiles were, in general, deeper than 850 m, in order to be consistent with XBT measurements and computations, only the upper 850 m of these profiles were used in this study. Monthly climatological T/S profiles below 850 m from the World Ocean Atlas 2013 [*Locarnini et al*., 2013] were used to complete the T/S profiles down to the ocean floor. Time series of T/S along four latitudes corresponding to those with higher correlation between SSHA and isotherm depths, 20°S, 25°S, 30°S, and 34.5°S, were then constructed for the period 1993–2011.

The MOC and MHT were separated into two components: geostrophic and ageostrophic (mainly Ekman) transports. Using the synthetic T/S profiles, the geostrophic velocities were computed from the thermal wind relationship with the reference level at 1000 m depth, which was chosen based on the availability of the absolute reference velocities from Argo drift data at the parking depth of 1000 m [*Katsumata and Yoshinari*, 2010]. These reference velocities are constant in time due to the limited available data. The zonal wind stress from the National Centers for Environmental Prediction/Department of Energy Reanalysis 2 was used here to compute the Ekman volume transport. The heat transport by the Ekman flow was computed using the SST. Following *Baringer and Garzoli* [2007], a velocity correction, of approximately 0.05 cm/s on average, was applied uniformly to the section to set the zero mass transport across the section in order to obtain meaningful estimates of MOC and MHT.

Examination of T/S fields from Argo floats indicates that similar to what was found for seasonal variations [*Dong et al*., 2014], the interannual variations in density and velocity are vertically coherent, although anomalies below 600 m are rather small. The methodology used here does not capture the interannual variations in MOC/MHT due to T/S changes below 850 m and of changes in the reference velocity. This results in an underestimation of the interannual variations in the geostrophic contribution to MOC. However, the velocity correction applied for zero mass transport is likely to counteract the underestimation errors from the missing variations below 850 m. A quantitative assessment of the errors is difficult due to the limited available data.

The approach taken in this study is different from *Willis* [2010] and *Frajka-Williams* [2015]. *Willis* [2010] combined altimeter data and Argo float measurements to derive dynamic height profiles in the North Atlantic and found that the MOC at 41°N estimated from those dynamic height profiles increased by 2.6 sverdrups (Sv) from 1993 to 2009, whereas *Frajka-Williams* [2015], using SSHA at 30°N, 70°W as a proxy for MOC at 26°N, suggested a decrease of 1.0 Sv from 1993 to 2014. In our study, temperature profiles are derived from altimeter data and used to compute the MOC/MHT in the South Atlantic. The MOC/MHT at 34.5°S has been studied using temperature profile measurements from the XBT transect AX18 [*Dong et al*., 2009], which are used to validate the methodology applied here.

3. Evaluation of the Methodology

In the South Atlantic, the longest available time series of MOC/MHT estimates are from the high-density XBT transect AX18 that runs zonally between Cape Town, South Africa, and Buenos Aires, Argentina, which forms the observational baseline for the evaluation in this study. To assess the methodology for deriving synthetic T/S profiles, synthetic temperature sections are constructed along the AX18 transect with the synthetic temperature profiles matching the location and time of XBT measurements for the 28 XBT realizations obtained during the period 2002–2011. A comparison between the AX18 observations and synthetic sections indicates

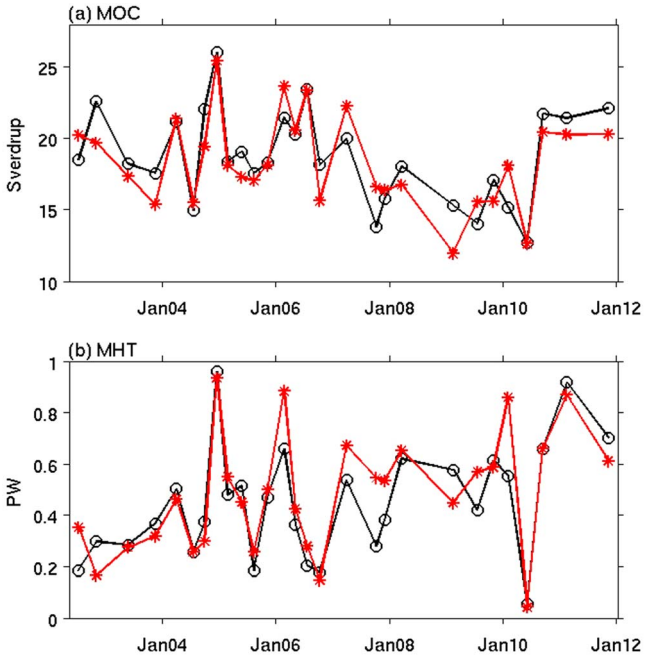

Figure 2. Comparison of the (a) MOC and (b) MHT along XBT transect AX18 estimated from the XBT measurements (black line) and the synthetic T/S profiles from altimeter SSHA (red line).

that the temperature differences above 200 m depth can be greater than 1°C, but mostly within ±0.5°C below 200 m, except near the boundaries (Figures 1c and 1d). The comparison of the MOC/MHT estimates from XBT transects with those from the synthetic sections (Figure 2) indicates that the biases in the synthetic profiles have a small impact on the MOC/MHT estimates.

The MOC/MHT estimates from synthetic T/S profiles capture the variations of the MOC/MHT from the AX18 transects, where the correlation coefficients between the XBT- and altimeter-derived MOC and MHT estimates are 0.86 and 0.87, respectively, well above the 95% significance level of 0.37. The time-mean MOC from altimeter-based (18.4 Sv) and XBT-based (18.8 Sv) estimates are very similar, with the altimeter-based estimate slightly lower. They also exhibit the same amount of variability with a standard deviation of 3.2 Sv. The time-mean MHT estimate from synthetic profiles (0.48 PW) is slightly higher than that obtained from the AX18 XBT transects (0.45 PW). However, their standard deviations are the same, of 0.23 PW. The differences of the XBT- and altimeter-derived MOC estimates are within ±3.0 Sv with a standard deviation of 1.7 Sv. The differences for MHT estimates are mainly within ±0.15 PW with a standard deviation of 0.11 PW. The differences in both the MOC and MHT are smaller than the seasonal variations in the MOC and MHT. The decorrelation time scale of the MOC/MHT differences is about 3 months based on the zero crossing of the autocorrelation, indicating that those differences do not influence the MOC/MHT variations on seasonal and interannual time scales. This comparison indicates that the altimeter measurements can be used to study the MOC and MHT changes on seasonal to interannual time scales in the South Atlantic.

4. Results and Discussion

4.1. Mean Values

Results from the altimeter-derived MOC at all four latitudes are summarized in Table 1, including their mean values, annual cycle, interannual variations, and contributions from the geostrophic and Ekman transports.

Table 1. Time-Mean, Peak-to-Peak Amplitude of the Annual Cycle, and Interannual Variations (Standard Deviation) of the Altimeter-Derived MOC at 20°S, 25°S, 30°S, and 34.5°S and Its Contributions From the Geostrophic and Ekman Components[a]

MOC (Sv)		20°S	25°S	30°S	34.5°S
Mean ± SD	Total	17.24 ± 1.72	18.24 ± 1.82	20.62 ± 2.17	19.45 ± 3.48
	Geostrophic	22.63 ± 1.22	21.11 ± 1.65	20.89 ± 1.83	16.62 ± 3.96
	Ekman	−5.39 ± 1.69	−2.87 ± 1.39	−0.27 ± 2.17	2.82 ± 3.12
Seasonal cycle (amplitude ± SD)	Total	2.83 ± 1.32	1.43 ± 1.72	4.32 ± 1.29	7.32 ± 2.19
	Geostrophic	2.13 ± 0.87	1.36 ± 1.46	3.84 ± 1.08	8.59 ± 2.11
	Ekman	2.36 ± 1.37	1.33 ± 1.27	4.08 ± 1.38	6.60 ± 1.74
Interannual variations (SD)	Total	1.37	1.74	1.34	2.27
	Geostrophic	0.90	1.51	1.11	2.19
	Ekman	1.42	1.30	1.46	1.84

[a]Units are in sverdrups.

The estimates obtained for the mean values of MOC (MHT) are 17.24 Sv (1.22 PW), 18.24 Sv (0.94 PW), 20.62 Sv (0.70 PW), and 19.45 Sv (0.49 PW) at 20°S, 25°S, 30°S, and 34.5°S, respectively, denoting a decrease of MOC and an increase in MHT toward the equator, which is consistent with the very few observational estimates available in the region [e.g., *Talley*, 2003; *Talley et al*., 2003]. Results also indicate that the mean geostrophic transport increases toward the equator from 16.62 Sv at 34.5°S to 22.63 Sv at 20°S. On the other hand, the mean Ekman transport decreases equatorward, with a positive value (northward) of 2.82 Sv at 34.5°S and reversing to negative values (southward) at 30°S, reaching the maximum southward transport of −5.39 Sv at 20°S. As found in previous studies [*Dong et al*., 2009; *Johns et al*., 2011], changes in MHT at each latitude are significantly correlated with changes in MOC on both seasonal and interannual time scales. Therefore, this work focuses only on the results for MOC. However, linear regression analysis indicates that the response of MHT to MOC varies with latitude, with a 1 Sv increase in MOC resulting in an increase in MHT of 0.033 ± 0.003 PW, 0.050 ± 0.003 PW, 0.022 ± 0.003 PW, and 0.040 ± 0.003 PW at 20°S, 25°S, 30°S, and 34.5°S, respectively.

4.2. Seasonal Variations

Consistent with what was previously found based on the MOC estimates using XBTs and Argo float data along 34.5°S, both the geostrophic and Ekman transports experience significant seasonal variations but with a phase difference. The geostrophic transport exhibits a peak-to-peak annual amplitude of 8.59 Sv, with the maximum occurring in March (20.68 Sv) and the minimum in August (12.09 Sv). On the other hand, the Ekman transport peaks in July (6.61 Sv) and reaches its minimum in February (0.01 Sv), exhibiting a weaker peak-to-peak annual cycle of 6.60 Sv. The amplitudes of the seasonal variations in both the geostrophic and Ekman components were somewhat higher than the values estimated from XBT transects and Argo measurements [*Dong et al*., 2009, 2014]. As a result, the seasonal variations in the total MOC are also higher (7.32 Sv) than the value of 6.42 Sv estimated from Argo data, with the maximum in May (23.40 Sv) and the minimum in October (16.08 Sv). However, the phases in the altimeter-derived MOC and in both the geostrophic and Ekman components are consistent with those estimated from Argo data [*Dong et al*., 2014]. One possibility for the stronger seasonal cycle derived from synthetic T/S estimates is that weekly altimeter data were used in this study, whereas a monthly climatology was used in the Argo float estimates [*Dong et al*., 2014]. This Argo monthly climatology was constructed from the gridded monthly T/S fields during 2004–2013, which were smoothed on a 3 month temporal scale [*Roemmich and Gilson*, 2009]. For example, the seasonal cycle of the MOC estimates is reduced to 6.66 Sv when the monthly climatology of synthetic T/S sections is generated with a 3 month smoothing. We note that the seasonal cycle in the XBT-based MOC estimates is much weaker, about 1.87 Sv. As discussed in *Dong et al*. [2014], the estimates from XBTs may be influenced by sampling aliasing in space and time, because the mean latitude of each AX18 transect varies between 30°S and 35°S, and the transect is only sampled every 3 months.

The altimeter-derived MOC at 30°S and 20°S also exhibits a statistically significant seasonal cycle (Figure 3), but relatively weaker compared to that at 34.5°S, with amplitudes of 4.32 Sv and 2.83 Sv, respectively. Similar to that at 34.5°S, both the geostrophic and Ekman components show significant seasonal variations. At 30°S, the amplitudes of the seasonal cycles in the geostrophic (3.84 Sv) and Ekman (4.08 Sv) transports are comparable, with a slightly higher value in the Ekman transport. The phases of the seasonal cycles in the MOC and in both the geostrophic and Ekman transports are the same as those at 34.5°S. The geostrophic and Ekman transports at 20°S also show similar amplitudes of the seasonal cycle, with values of 2.13 Sv and 2.36 Sv, respectively. The phase in the MOC is more or less consistent with those at 30°S and 34.5°S. However, the phases in the geostrophic and Ekman components are different from other latitudes. The geostrophic component reaches its maximum in June and minimum in February (Figure 3). The maximum Ekman transport occurs in January and the minimum in August. Different from the other three latitudes, the MOC and the contributions from the geostrophic and Ekman transports at 25°S do not show a statistically significant seasonal cycle.

4.3. Interannual Variability

To investigate the interannual variations of the altimeter-derived MOC, a 13 month running average was applied to the anomalous MOC time series. Here the anomalous MOC refers to the MOC after the monthly average is removed. The interannual variations in the MOC at all four latitudes are comparable (Figure 4), with

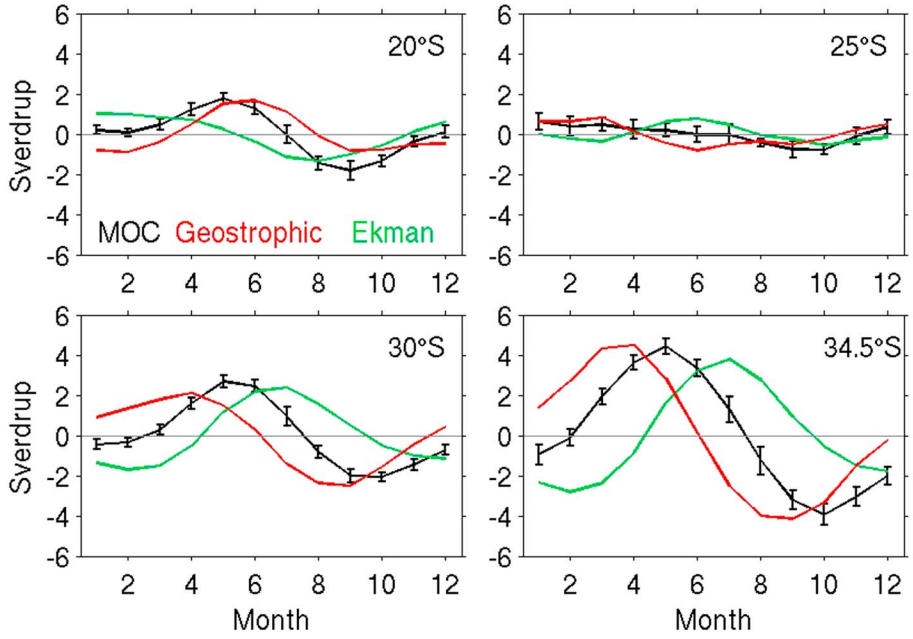

Figure 3. Seasonal variations of the MOC (black) and contributions from the geostrophic (red) and Ekman (green) components estimated from the synthetic T/S profiles at 20°S, 25°S, 30°S, and 34.5°S, respectively. The time-mean values for the total MOC and each component have been removed. Error bars indicate the standard error.

the majority of the MOC anomalies varying within ±1.0 Sv. At all latitudes, the anomalous MOC is dominated by negative values during 1994–2000 and 2010–2011 and positive values during 2001–2010.

The interannual variations in the MOC from 30°S to 20°S are significantly correlated, with correlations varying from 0.60 to 0.71 between any two pairs exceeding the 95% significance level of 0.45. However, the correlations of the MOC at 34.5°S with those at the other three latitudes are all below the 95% significance level.

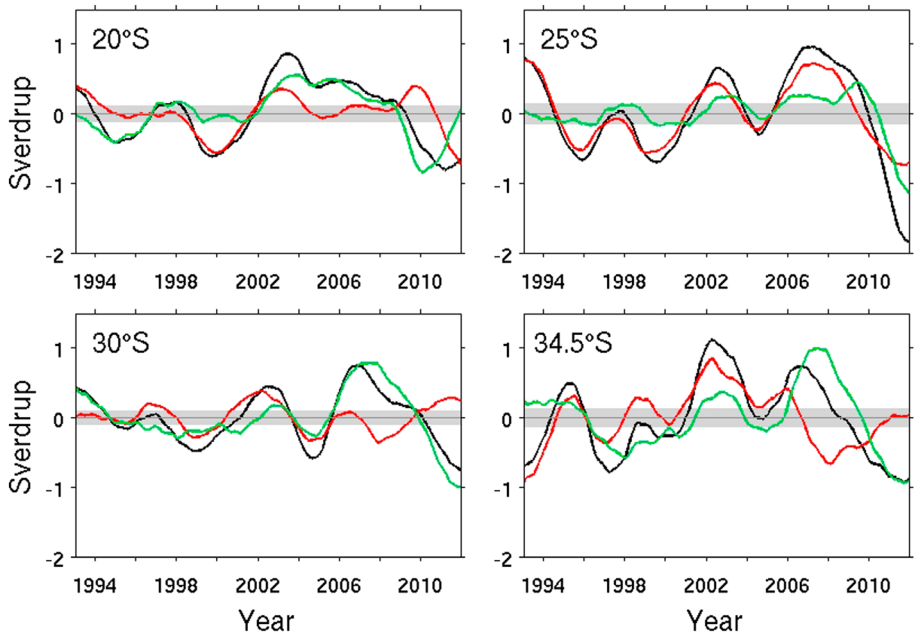

Figure 4. Interannual variations of the MOC (black) and contributions from the geostrophic (red) and Ekman (green) components at 20°S, 25°S, 30°S, and 34.5°S, respectively. The gray shading denotes the range where anomalies are not significantly different from zero.

Many factors can contribute to this low correlation. The ocean circulation pattern in the South Atlantic near 34.5°S is very complex, with the Brazil and Benguela Currents contributing to the MOC variability [*Dong et al.*, 2009]. In addition, the Agulhas leakage, which has very large year-to-year variations, may also play a large role in the MOC variability at 34.5°S.

4.4. Dominance of Geostrophic and Ekman Components

Results indicate that the dominance of the geostrophic and Ekman transports is different at different latitudes and time periods. For example, at 34.5°S and 30°S, the geostrophic transport dominates the interannual variability of the MOC before 2006, while the Ekman transport dominates after 2006. On the other hand, at 25°S the geostrophic transport plays a larger role throughout the entire study period. The interannual variations in the Ekman transport are relative weak except during the last 3 years. Whereas at 20°S, the Ekman component plays a large role except during the period 1999–2002 when the geostrophic transport experiences large anomalies.

5. Conclusions

This study represents the first effort to estimate a time series of the MOC in the South Atlantic between 20°S and 34.5°S, from even before the in situ observing system was in place, showing the key value of integrating satellite and hydrographic measurements. Also, results obtained from this work show the importance of maintaining sustained observations, such as those from the XBT transect AX18, which are critical to validate altimetry estimates. The altimeter-derived MOC/MHT estimates along the XBT transects capture the changes of the MOC/MHT derived from XBT measurements, indicating that the altimetry data can be used to study the MOC and MHT in the South Atlantic. The methodology presented here also serves to estimate the SAMOC and MHT in near real time, which can be used to validate and initialize forecast models. Limitations of this methodology may include potential time dependence of the T/S relationships, and analysis of long-period climate trends may not hold if these relationships change with time. The main results obtained in this work showed that the geostrophic (Ekman) component of the MOC is dominant before (after) 2006 and that since 2010 the MOC has exhibited low values when compared to the 1993–2011 mean values.

Our future work will include comparisons of MOC/MHT estimates from other observational platforms, assessment of the impact of the boundary currents and interior region, and evaluation of climate models in simulating MOC/MHT in the South Atlantic.

Acknowledgments

The authors thank Ricardo Domingues in deriving the statistical relationships between SSHA and depth of isotherms. World Ocean Atlas 2013 is from http://www.nodc.noaa.gov/OC5/woa13/. Altimeter data are available at http://www.aviso.altimetry.fr/en/data/data-access.html. The velocity at 1000 m depth from Argo floats is from http://apdrc.soest.hawaii.edu/projects/Argo/data/trjctry/. This work was supported by NASA grant NNH13AW33I and NOAA grant NA10OAR4310206 and also by the NOAA Atlantic Oceanographic and Meteorological Laboratory (AOML). This research was carried out in part under the auspices of the Cooperative Institute for Marine and Atmospheric Studies of the University of Miami and NOAA, cooperative agreement NA10OAR4320143.

The Editor thanks two anonymous reviewers for their assistance in evaluating this paper.

References

Baringer, M. O., and S. L. Garzoli (2007), Meridional heat transport determined with expendable bathythermographs. Part I: Error estimates from model and hydrographic data, *Deep Sea Res., Part I*, *54*(8), 1390–1401.

Biastoch, A., C. W. Boning, and J. R. E. Lutjeharms (2008), Agulhas leakage dynamics affects decadal variability in Atlantic overturning circulation, *Nature*, *456*, 489–492, doi:10.1038/nature07426.

Cunningham, S. A., et al. (2007), Temporal variability of the Atlantic Meridional Overturning Circulation at 26.5°N, *Science*, *317*, 935–938, doi:10.1126/science.1141304.

Dong, S., S. L. Hautala, and K. A. Kelly (2007), Interannual variations in upper-ocean heat content and heat transport convergence in the western North Atlantic, *J. Phys. Oceanogr.*, *37*, 2682–2697, doi:10.1175/2007JPO3645.1.

Dong, S., S. L. Garzoli, M. O. Baringer, C. S. Meinen, and G. J. Goni (2009), The Atlantic Meridional Overturning Circulation and its northward heat transport in the South Atlantic, *Geophys. Res. Lett.*, *36*, L20606, doi:10.1029/2009GL039356.

Dong, S., M. O. Baringer, G. J. Goni, C. S. Meinen, and S. L. Garzoli (2014), Seasonal variations in the South Atlantic Meridional Overturning Circulation from observations and numerical models, *Geophys. Res. Lett.*, *41*, 4611–4618, doi:10.1002/2014GL060428.

Ducet, N., P.-Y. Le Traon, and G. Reverdin (2000), Global high resolution mapping of ocean circulation from TOPEX/POSEIDON and ERS-1 and -2, *J. Geophys. Res.*, *105*, 19,477–19,498.

Enfield, D. B., A. M. Mestas-Nunez, and P. J. Trimble (2001), The Atlantic Multidecadal Oscillation and its relation to rainfall and river flows in the continental U.S, *Geophys. Res. Lett.*, *28*(10), 2077–2080, doi:10.1029/2000GL012745.

Frajka-Williams, E. (2015), Estimating the Atlantic overturning at 26°N using satellite altimetry and cable measurements, *Geophys. Res. Lett.*, *42*, 3458–3464, doi:10.1002/2015GL063220.

Garzoli, S. L., M. O. Baringer, S. Dong, R. C. Perez, and Q. Yao (2013), South Atlantic meridional fluxes, *Deep Sea Res., Part I*, *71*, 21–32, doi:10.1016/j.dsr.2012.09.003.

Goni, G. J., F. Bringas, and P. N. DiNezio (2011), Observed low frequency variability of the Brazil Current front, *J. Geophys. Res.*, *116*, C10037, doi:10.1029/2011JC007198.

Goni, G., S. Kamholz, S. Garzoli, and D. Olson (1996), Dynamics of the Brazil-Malvinas Confluence based on inverted echo sounders and altimetry, *J. Geophys. Res.*, *101*(C7), 16,273–16,289, doi:10.1029/96JC01146.

Johns, W. E., et al. (2011), Continuous, array-based estimates of Atlantic Ocean heat transport at 26.5°N, *J. Clim.*, *24*, 2429–2449.

Katsumata, K., and H. Yoshinari (2010), Uncertainties in global mapping of Argo drift data at the parking level, *J. Oceanogr.*, *66*, 553–569.

Kelly, K. A., L. Thompson, and J. Lyman (2014), The coherence and impact of meridional heat transport anomalies in the Atlantic Ocean inferred from observations, *J. Clim.*, *27*, 1469–1487, doi:10.1175/JCLI-D-12-00131.1.

Lee, S.-K., W. Park, E. Van Sebille, M. O. Baringer, C. Wang, D. B. Enfield, S. Yeager, and B. P. Kirtman (2011), What caused the significant increase in Atlantic ocean heat content since the mid-20th century?, *Geophys. Res. Lett.*, *38*, L17607, doi:10.1029/2011GL048856.

Locarnini, R. A., et al. (2013), in *World Ocean Atlas 2013, Volume 1: Temperature*, *NOAA Atlas NESDIS*, vol. 73, edited by S. Levitus and A. Mishonov, 40 pp., NOAA, Silver Spring, Md.

Mayer, D., R. Molinari, M. Baringer, and G. Goni (2001), Transition regions and their role in the relationship between sea surface height and subsurface temperature structure in the Atlantic Ocean, *Geophys. Res. Lett.*, *28*, 3943–3946.

Meinen, C. S., S. Speich, R. C. Perez, S. Dong, A. R. Piola, S. L. Garzoli, M. Baringer, S. Gladyshev, and E. Campos (2013), Temporal variability of the Meridional Overturning Circulation at 34.5°S: Results from two pilot boundary arrays in the South Atlantic, *J. Geophys. Res. Oceans*, *118*, 6461–6478, doi:10.1002/2013JC009228.

Roemmich, D., and J. Gilson (2009), The 2004–2008 mean and annual cycle of temperature, salinity, and steric height in the global ocean from the Argo Program, *Prog. Oceanogr.*, *82*, 81–100.

Sijp, W. P., and M. H. England (2008), The effect of a northward shift in the southern hemisphere westerlies on the global ocean, *Progress Oceanogr.*, *79*, 1–19.

Sijp, W. P., and M. H. England (2009), Southern hemisphere westerly wind control over the ocean's thermohaline circulation, *J. Clim.*, *22*, 1277–1286.

Smeed, D. A., et al. (2014), Observed decline of the Atlantic Meridional Overturning Circulation 2004–2012, *Ocean Sci.*, *10*, 29–38, doi:10.5194/os-10-29-2014.

Stommel, H. (1961), Thermohaline convection with two stable regimes of flow, *Tellus*, *13*, 224–230, doi:10.1111/j.2153-3490.1961.tb00079.x.

Stouffer, R. J., J. Yin, and J. M. Gregory (2006), Investigating the causes of the response of the thermohaline circulation to past and future climate changes, *J. Clim.*, *19*(8), 1365–1387.

Sun, C., et al. (2010), The data management system for the global temperature and salinity profile programme, in *Proceedings of OceanObs.09: Sustained Ocean Observations and Information for Society*, vol. 2, edited by J. Hall, D. E. Harrison, and D. Stammer, ESA Publ. WPP-306, Venice, Italy, doi:10.5270/OceanObs09.cwp.86.

Sutton, R. T., and D. L. R. Hodson (2005), Atlantic Ocean forcing of North American and European summer climate, *Science*, *309*, 115–118, doi:10.1126/science.1109496.

Talley, L. D. (2003), Shallow, intermediate, and deep overturning components of the global heat budget, *J. Phys. Oceanogr.*, *33*, 530–560.

Talley, L. D., J. L. Reid, and P. E. Robbins (2003), Data-based meridional overturning streamfunctions for the global ocean, *J. Clim.*, *16*, 3213–3226.

Toggweiler, J. R., and B. L. Samuels (1993), Is the magnitude of the deep outflow from the Atlantic Ocean actually governed by Southern Hemisphere winds? in *The Global Carbon Cycle*, edited by M. Heimann, pp. 303–331, Springer, Berlin.

Toggweiler, J. R., and B. L. Samuels (1995), Effect of Drake Passage on the global thermohaline circulation, *Deep Sea Res., Part I*, *42*(4), 477–500.

Vellinga, M., and R. A. Wood (2002), Global climatic impacts of a collapse of the Atlantic thermohaline circulation, *Clim. Change*, *54*, 251–267.

Weaver, A. J., and T. M. C. Hughes (1992), Stability and variability of the thermohaline circulation and its link to climate, *Trends Phys. Oceanogr.*, *1*, 15–70.

Willis, J. (2010), Can in situ floats and satellite altimeters detect long-term changes in Atlantic Ocean overturning, *Geophys. Res. Lett.*, *37*, L06602, doi:10.1029/2010GL042372.

Zhang, D., R. Msadek, M. J. McPhaden, and T. Delworth (2011), Multidecadal variability of the North Brazil Current and its connection to the Atlantic Meridional Overturning Circulation, *J. Geophys. Res.*, *116*, C04012, doi:10.1029/2010JC006812.

Zhang, R., and T. L. Delworth (2006), Impact of Atlantic multidecadal oscillations on India/Sahel rainfall and Atlantic hurricanes, *Geophys. Res. Lett.*, *33*, L17712, doi:10.1029/2006GL026267.